NASA TECHNICAL NOTE

NASA TN D-7987

EXPERIMENTALLY DETERMINED STIFFNESS AND DAMPING OF AN INHERENTLY COMPENSATED AIR SQUEEZE-FILM DAMPER

Robert E. Cunningham

Lewis Research Center
Cleveland, Ohio 44135

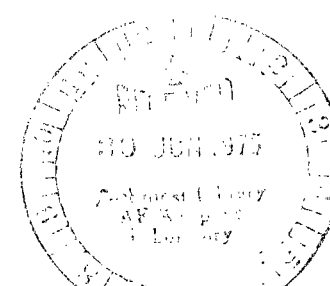

NATIONAL AERONAUTICS AND SPACE ADMINISTRATION • WASHINGTON, D. C. • JUNE 1975

1. Report No.	2. Government Accession No.	3. Recipient's Catalog No.
NASA TN D-7987		

4. Title and Subtitle
EXPERIMENTALLY DETERMINED STIFFNESS AND DAMPING OF AN INHERENTLY COMPENSATED AIR SQUEEZE-FILM DAMPER

5. Report Date
June 1975

6. Performing Organization Code

7. Author(s)
Robert E. Cunningham

8. Performing Organization Report No.
E-8207

9. Performing Organization Name and Address
Lewis Research Center
National Aeronautics and Space Administration
Cleveland, Ohio 44135

10. Work Unit No.
505-04

11. Contract or Grant No.

12. Sponsoring Agency Name and Address
National Aeronautics and Space Administration
Washington, D.C. 20546

13. Type of Report and Period Covered
Technical Note

14. Sponsoring Agency Code

15. Supplementary Notes

16. Abstract

Experimental values of damping and stiffness were determined for an externally pressurized, inherently compensated, compressible squeeze-film damper up to excitation frequencies of 36 000 cycles per minute. Experimental damping values were higher than theory predicted at low squeeze numbers and less than predicted at high squeeze numbers. Experimental values of air film stiffness were less than theory predicted at low squeeze numbers and much greater at higher squeeze numbers. Results also indicated sufficient damping is available to attenuate amplitudes and forces at the critical speed when using three such dampers in the flexible support system of a small, lightweight turborotor.

17. Key Words (Suggested by Author(s))	18. Distribution Statement
Air bearings; Externally pressurized; Damping; Squeeze film; Vibration; Rotor dynamics	Unclassified - unlimited STAR Category 07 (rev.)

19. Security Classif. (of this report)	20. Security Classif. (of this page)	21. No. of Pages	22. Price*
Unclassified	Unclassified	31	$3.75

* For sale by the National Technical Information Service, Springfield, Virginia 22151

EXPERIMENTALLY DETERMINED STIFFNESS AND DAMPING OF AN INHERENTLY COMPENSATED AIR SQUEEZE-FILM DAMPER

by Robert E. Cunningham

Lewis Research Center

SUMMARY

Experiments were conducted to determine the dynamic characteristics of damping and stiffness of an externally pressurized, inherently compensated, compressible squeeze-film damper. Each damper was 76.2 millimeters (3 in.) square and contained 20 equally spaced feed holes 1.5 millimeters (0.059 in.) in diameter. Results were obtained at clearances of 63.5, 50.8, 38.1, and 25 micrometers (0.0025, 0.002, 0.0015, and 0.001 in.), at supply pressure ratios of 2 and 3, and for excitation frequencies to 36 000 cycles per minute. The test apparatus consisted of three such dampers arranged in an equilateral, triangular pattern.

Experimental values of the squeeze-film damping when compared with a small pressure perturbation analysis were much greater than predicted at low squeeze numbers (<20) and slightly less than predicted at higher squeeze numbers (>20).

It was determined for limited applications requiring only light damping in a flexible bearing support that a gas squeeze-film damper similar to the type investigated could supply approximately the same amount of damping as could the previously designed oil squeeze-film damper. The clearances in the gas squeeze-film damper would have to be much smaller to obtain the same magnitude of damping - that is, 38.1 micrometers (0.0015 in.) for the air as compared to 127 micrometers (0.005 in.) for the oil.

Experimental stiffness values when compared to plotted results of the small perturbation analysis were much less than predicted for low squeeze numbers and much greater for high squeeze numbers.

INTRODUCTION

Small, lightweight, high speed turbomachines are being designed in increasing numbers. To insure the safe operation of these machines and to provide reasonable

operating longevity, considerable attention must be given to the interaction of the rotor and its bearing supports.

The rotors of these machines can be designed to operate either as rigid or flexible members. The bearing supports can be an integral part of the machine frame, having a stiffness of the same order of magnitude as the rolling element bearings, or they can be flexible, having a stiffness much less than that of the bearings. These so-called "soft" supports serve two functions:

(1) They can suppress the system rigid body critical speeds well below the operating range.

(2) They can attenuate the forces transmitted to the bearings (ref. 1).

Currently, a number of production turbojet engines are using a type of cantilevered "squirrel cage" spring to support the bearings. Once support flexibility is introduced, however, it becomes necessary to also provide a damping mechanism. Flexibility without damping can produce a system highly sensitive to shock as in the case of suddenly applied unbalance loads (ref. 1).

The literature on rotor dynamics contains many reports which treat the dynamic response of a rigid rotor in rigid supports. References 2 and 3 treat the more complex problem of an elastic rotor in elastic, damped supports. With the aid of the computer programs developed in these analyses, the machinery designer can, with some degree of confidence, predict the response of an unbalanced rotor to assigned values of support stiffness and damping. To build into the machine just the correct amount of stiffness and damping is, however, a much more difficult task.

More often than not, compromise solutions are necessary to satisfy the various sets of operating conditions encountered in high speed machinery. For example, to guard against bearing failures due to large transient overloads, much higher damping in the supports is used than is necessary to operate through a critical speed at nominal unbalance conditions. The greater damping can, at operating speeds, transmit larger forces to the bearings and thus result in their premature failure (ref. 1).

Some of the more conventional methods of obtaining support damping (lubricating oils and elastomers) have reduced effectiveness when exposed to high temperatures in an actual machine. Elastomers used as springs and/or dampers can have their dynamic properties significantly altered by high temperatures, either self-induced or from adjacent hot parts.

The high temperatures in bearing compartments can change the viscosity of lubricating oil and thus result in a change in the damping coefficient. In certain applications the temperatures may be high enough to even prohibit the use of such oils as damper fluids.

For these reasons one is led to consider an externally pressurized, air squeeze-film bearing to provide the flexibility and damping needed to attenuate the forces transmitted to the supports in certain high temperature applications.

The gas bearing literature contains a number of reports which investigate the characteristics of hydrodynamic, compressible, squeeze-film bearings (refs. 4 and 5). There are also several reports on the dynamic characteristics of the externally pressurized bearing (refs. 6 to 8). Reference 9 treats the dynamic characteristics of an inherently compensated, multiple feed hole, circular gas thrust bearing. The research reported in references 7 and 10 includes experimental data on the dynamic properties of externally pressurized journal bearings.

To be able to use such a bearing as a flexible support, the stiffness and damping properties must be predictable. To date, only a small amount of experimental data is available to compare with the analyses. One objective of this investigation is to determine the stiffness and damping of an externally pressurized, inherently compensated, air film damper at clearances of 63.5, 50.8, 38.1, and 25 micrometers (0.0025, 0.002, 0.0015, and 0.001 in.) for supply pressure ratios of 2 and 3 and excitation frequencies to 36 000 cycles per minute. The results are compared to a small pressure perturbation linearized analysis for a multiple feed hole, inherently compensated, gas film damper (ref. 11).

A second objective of this investigation is to determine the feasibility of using an arrangement of three externally pressurized bearings as a flexible damped support whose dynamic characteristics can be readily altered to attenuate amplitudes of motion and transmitted forces while the rotor operates through its critical speeds.

The polygonal arrangement of the three rectangular shaped, externally pressurized pads used as a flexible, damped support lends itself to ease of clearance adjustment. This would be very difficult to do with a circular bearing. The rectangular pads arranged in a triangle also prevent rotation without using anti-rotation pins, etc. Finally, the pressure in each individual pad can be regulated to obtain the amount of stiffness necessary to satisfy the rotor unbalance forces at any particular speed. This would also be difficult to do in a support with circular geometry. Because of the unique features embodied in this concept, a patent disclosure has been filed.

SYMBOL LIST

A ratio of center region length to total pad length, ℓ/L

B squeeze film damping coefficient, N-sec/m ((lb-sec)/in.)

$\overline{B}$ dimensionless damping, $Bh^3/\mu L^4$

C_D orifice discharge coefficient

d_o orifice diameter, mm (in.)

e housing peak to peak amplitude, mm (in.)

F rotating unbalance force, N (lb)

f	coefficient representing integral of pressure gradient along source boundary, dimensionless
g	acceleration of gravity, m/sec^2 ($in./sec^2$)
h	film thickness, mm (in.)
K	squeeze film stiffness, N/m, (lb/in.)
K	dimensionless stiffness, $Kh/\{L^2P_a[(P_s/P_a) - 1]\}$
k	adiabatic gas exponent
ℓ	center region length, m (in.)
L	damper pad length, m (in.)
M	housing mass, kg ($lb\text{-}sec^2/in.$)
m	unbalance mass, kg ($lb\text{-}sec^2/in.$)
N	turbine speed, rev/min
n	number of orifices
P_a	ambient pressure, N/m^2 ($lb/in.^2$ abs)
P_s	supply pressure, N/m^2 ($lb/in.^2$ abs)
R	gas constant, J/(kg)(K) (in.-lb/(lb)(^oR))
r	distance to unbalance weight, m (in.)
T	temperature, K
t	time, sec
U	unbalance, kg-m (oz-in.)
W	housing weight, kg (lb)
w	unbalance weight, kg (lb)
x, y, z	coordinate axes
Λ	restrictor coefficient, $6\mu C_D n\pi d_o \left[2kRT/(k - 1)^{1/2}\right] \Big/ P_s h^2_f$
μ	absolute viscosity, $N\text{-}sec/m^2$ ($lb\text{-}sec/in.^2$)
σ	squeeze number, $12\mu\omega L^2/h^2P_a$
φ	phase angle, deg
ω	angular velocity, rad/sec
ω_c	angular velocity at resonance, rad/sec

Subscript:

e	error value

APPARATUS

Mechanical Components

The experimental results presented in this report were obtained using the test apparatus shown schematically in figure 1 and photographically in figures 2 and 3. An equilateral triangular damper housing having three precision ground and lapped faces is located by three externally pressurized gas damper pads. These pads are 7.62 millimeters (3 in.) square and contain twenty 1.50-millimeter- (0.059-in.-) diameter feed holes arranged in a square pattern (fig. 4). Two of the pads are rigidly attached to a base plate while the third is mounted on a micrometer slide permitting adjustment of the gas film clearance in all three damper pads. Each pad has its own air supply which can be regulated independently. This pressure was measured by Bourdon tube type gages. The housing was supported vertically by a pocketed externally pressurized thrust bearing.

An air driven turbine wheel is mounted on the inside of a circular cavity in the housing whose plane is perpendicular to the pad faces (see fig. 1). The turbine rotates on a ball bearing and contains a small unbalance moment of 3.99×10^{-5} kilogram-meter (0.0553 oz-in.). This amount of unbalance was measured on a two plane dynamic balancing machine. The rotating turbine wheel produces a harmonic exciting force acting normal to each gas bearing surface; this is shown schematically in figure 5.

INSTRUMENTATION

The instrumentation used to obtain the experimental results is shown schematically in figure 6. Two noncontacting, proximity measuring probes are mounted flush with the surfaces of each of the three pads. The output voltage from the probes is proportional to this displacement. This signal is amplified, fed into a tracking filter from where it goes to a peak to peak measuring voltmeter, and finally displayed on an X-Y-Y' plotter.

A magnetic probe mounted over the turbine wheel produces a conditioned voltage pulse once per revolution when triggered by a single narrow tooth on the turbine wheel located at the same angle as the unbalance weight. This pulse, in addition to measuring the angular velocity of the turbine wheel, provides the reference for measuring phase angle. This is the angle between the force and displacement vectors as measured by an electronic phase meter. The output from the phase meter is then fed to the Y'-axis of the X-Y-Y' plotter. A dynamic input sine converter (DISC) takes the repetitive pulse and converts it to a dc voltage which is proportional to frequency. This signal is then applied to the X-axis of the plotter where housing amplitude and phase angle are automatically plotted against rotor frequency.

The DISC is also used to convert the dc pulse from the magnetic pickup to a sinusoidally varying output which in turn is used to drive the carrier generator of the tracking filter. The tracking filter has both a 10- and 20-hertz bandpass filter, either one of which can be used. Amplitude and phase can also be measured on a cathode ray oscilloscope (CRO). The reference pulse relative to the sinusoidal motion of the housing is shown in figure 7; the photographs of the CRO screen were taken during a test run.

PROCEDURE

Initial Assembly

In order to achieve the best alinement possible between the damper faces and the triangular housing, the following steps were taken in the fabrication and initial assembly of these components.

The three faces of the damper housing were ground and lapped to within ±5 micrometers (±0.0002 in.) of a true equilateral triangle. In addition, each face was held within three helium light bands of being optically flat. These same tolerances were also held on a circular externally pressurized thrust bearing and on the mating surface at the bottom of the triangular damper housing.

Before attaching any of three damper pads to the base plate, the pads were first moved into contact with the triangular housing after having positioned 10-micrometer- (0.0004-in. -) thick paper shims at each of the four corners of each pad. Shims were placed, if required, between the base plate and the base of each externally pressurized pad until equal tension was achieved on each of the paper shims. The pads were then carefully bolted down and doweled in place. The same procedure was used to insure the parallelism of the adjustable pad with its mating surface on the housing when bolted to the micrometer adjustable slide.

PRETEST

Before each test the clearance between each bearing and its respective mating surface was adjusted. First, air was supplied to the thrust bearing at 55.2×10^4 newtons per square meter (80 psig in the plenum) to lift the housing from the thrust bearing surface. When the housing floated freely at approximately a 38.1-micrometer (0.0015-in.) clearance, the adjustable pad was moved in until metal to metal contact was made on all three pads. The two capacitance probes in each pad were adjusted to approximately 50.8 micrometers (0.002 in.) below the surface of each pad. This was determined by the output

voltage from the probes as read on a digital voltmeter. This value was recorded and became the zero clearance reading.

The adjustable pad was then moved back with the micrometer slide until a specific clearance was achieved. The air supply was then turned on to each pad and the pressure in each plenum adjusted to the same value. The clearance in each pad was checked on the voltmeter and recorded. Stops on the adjustable damper pad were then positioned so that the play in the micrometer slide did not allow any movement of this pad. The average clearance was within 5 percent for all three pads.

The next steps involved calibrating the instrumentation shown in figure 6. Prior to each test the two tracking channel bandpass filters of 10 and 20 hertz were calibrated using an audio oscillator monitored by an electronic counter. The amplitude and phase axes were then calibrated using the same audio oscillator, dynamic sine converter, and dc peak to peak reading voltmeter.

TEST

The air supply valve on a speed controller was opened to provide drive air to the unbalanced turbine wheel. The plotter was turned on to record the amplitude and phase of the resulting housing motion relative to a single pad over a range of frequencies to 36 000 cycles per minute. A cathode ray oscilloscope was also used to monitor both the amplitude and phase as shown in figure 7. The test clearance and zero clearance readings were again checked at the conclusion of each test.

RESULTS AND DISCUSSION

The experimental results of this investigation are presented in figures 8 to 15 and are compared to the theoretical results obtained in the small pressure perturbation linearized analysis of reference 11.

Experimental values of damping and stiffness were obtained from the equation of motion for a damped single degree of freedom spring mass system subjected to a harmonic exciting force. The following force displacement equation is from reference 12 and pertains to the system under investigation:

$$M\left[e\omega^2 \sin(\omega t - \varphi)\right] - \frac{3B}{2}\left[e\omega \sin\left(\omega t - \varphi + \frac{\pi}{2}\right)\right] - \frac{3K}{2}\left[e \sin(\omega t - \varphi)\right] + F \sin \omega t = 0 \quad (1)$$

From this equation these vector diagrams can be constructed.

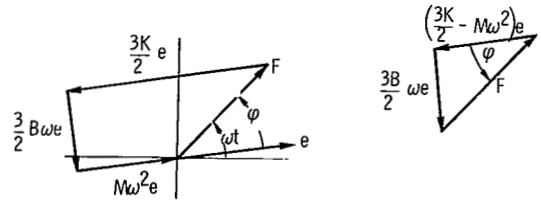

Damping and stiffness coefficients are solved for as follows using the vector diagram on the right:

Damping coefficient:

$$B = \frac{2F \sin \varphi}{3e\omega} \qquad \frac{\text{N-sec}}{\text{M}} \left(\frac{\text{lb - sec}}{\text{in.}} \right) \tag{2}$$

Stiffness coefficient:

$$K = \frac{2F \cos \varphi}{3e} + \frac{2M\omega^2}{3} \qquad \frac{\text{N}}{\text{M}} \left(\frac{\text{lb}}{\text{in.}} \right) \tag{3}$$

The measured variables were peak to peak amplitude, phase angle φ, and frequency ω of the exciting force F which was equal to the turbine frequency.

Since there are three pads, there are actually three equivalent springs and dampers. However, it is easily verified that when all pads are identical the spring and damping constants in any direction are equal to (3/2)K and (3/2)B, respectively, where K and B are constants for a single pad. Since the constants are directionally uniform, a rotating load, as applied in the apparatus, produces a circular motion. This was verified by accelerometers mounted orthogonally on the damper housing. The accelerometer signal, displayed on an X-Y curve tracing oscilloscope, showed a circular orbit.

Figure 8 is for an actual plot of the housing peak to peak motion and the phase angle as a function of excitation frequency. Figure 8(a) is at a clearance of 63.5 micrometers (0.0025 in.) and shows a large buildup in amplitude at the resonant frequency; this indicates very light damping. Figure 8(b) is at a clearance of 25 micrometers (0.001 in.) where no peak amplitude occurs at resonance; this indicates the presence of much greater damping.

In order to compare the experimental values of damping and stiffness with the theoretical values as plotted in reference 11, the data were put in nondimensional form by the following equations:

Dimensionless damping:

$$\overline{B} = \frac{Bh^3}{\mu L^4} \tag{4}$$

Dimensionless stiffness:

$$\overline{K} = \frac{Kh}{L^2 P_a \left[(P_s/P_a) - 1 \right]} \tag{5}$$

Squeeze number:

$$\sigma = \frac{12 \mu \omega L^2}{h^2 P_a} \tag{6}$$

DAMPING

Figure 9 is for a pressure ratio of 2. The theoretical dimensionless damping remains relatively constant through squeeze numbers of approximately 20; beyond 20 there is a pronounced reduction in damping. For very high squeeze numbers the predicted damping diminishes to extremely small values (ref. 11). At an initial clearance of 63.5 micrometers (0.0025 in.) the experimental data from six tests (fig. 9(a)) when compared with theory show that the damping is much higher than predicted. In addition, the data show considerable scatter. This is probably due to the fact that the initial clearance h was reset between tests and that tests at the same clearance were not run consecutively. For successively smaller initial clearances, figures 9(b) to (d) show fair agreement with theory. At values of 38.1 and 25 micrometers (0.0015 and 0.001 in.) (figs. 9(c) and (d)), the theory overpredicts throughout the range of squeeze numbers investigated. Similarly, at a supply pressure ratio of 3 (figs. 10(c) to (d)) the experimental results exhibit the same trend with slightly better agreement for clearances of 38.1 and 25 micrometers (0.0015 and 0.001 in.) (figs. 10(c) and (d)).

Figures 11 and 12 are cross plots of the dimensional damping coefficient B against initial film clearance at a squeeze number σ of 10 and supply pressure ratios P_s/P_a of 2 and 3, respectively. A squeeze number of 10 was chosen for this comparison because the damping data were taken at this value for all values of clearances tested. These two figures show how rapidly the squeeze film damping increases with decreasing clearance. The actual measured damping is less than predicted at clearances up to 50.8 micrometers (0.0020 in.) at $P_s/P_a = 2$ and up to 45.7 micrometers (0.0018 in.) at $P_s/P_a = 3$; the actual damping becomes greater than predicted at clearances larger

than these. These damping curves are typical of externally pressurized gas bearings, and similar results are shown in reference 7.

STIFFNESS

Gas film stiffness in nondimensional form is plotted as a function of squeeze number in figures 13 and 14. The experimental values are compared with the theory of reference 11. Agreement between the experimental data and the theory is poor at the higher clearances. For a clearance of 25 micrometers (0.001 in.) the agreement is fair at supply pressure ratios of 2 and 3. Values of stiffness increase at a much more rapid rate for increasing squeeze numbers than the theory predicts. At low squeeze numbers the measured stiffness is much less than theory predicts except at a clearance of 25 micrometers (0.001 in.) and a supply pressure ratio of 2.

In figure 15 theoretical and measured stiffnesses (figs. 13 and 14) are plotted as functions of the initial clearance at a squeeze number of 10 and for supply pressure ratios of 2 and 3. Experimental values of squeeze film stiffnesses ranged from a high of 143.7×10^5 newtons per meter (82 000 lb/in.) at a supply pressure ratio of 3 and a clearance of 63.5 micrometers (0.0025 in.) to a low of 13.1×10^5 newtons per meter (7500 lb/in.) at a supply pressure ratio of 2 and a clearance of 25 micrometers (0.001 in.).

ERROR ANALYSIS

The dynamic characteristics of a gas film, specifically stiffness and damping, cannot be measured directly. Values of these coefficients must be calculated from the values that can be measured directly - these being displacement, phase angle, frequency, and initial clearance.

A number of different sensors and instruments are necessary to measure these variables and, of course, each is subject to error. The following are typical accuracies of instruments used as obtained from manufacturers' operating manuals:

	Percent error
Proximity sensor output	±2.6
Digital voltmeter	±3.0
Amplifier	±.01
Dynamic input sine converter	±.25
Tracking filter	±2.0
Phase meter	.08
Peak to peak dc voltmeter	±4.0
X-Y-Y' plotter	±.2

In addition to the errors inherent in the instrumentation, there is a probable misalinement error of ±0.0002 inch.

The following sample calculations illustrate the potential error in the measured values of amplitude of housing motion, frequency of exciting force, the phase angle, and initial clearance setting. The measured values were at test conditions of $P_s/P_a = 2$ and h = 63.5 micrometers (0.0025 in.).

(1) Potential error in peak to peak amplitude - dependent on proximity sensor, amplifier, tracking filter, peak to peak voltmeter, and X'-Y-Y' plotter (observed value, e = 13.46 μm (0.00053 in.)):

$$e_e = 13.46\ \mu m\ (0.00053\ in.) \times \pm 0.088 = \pm 1.18\ \mu m\ (4.63 \times 10^{-5}\ in.)$$

$$e_e = 13.36 \pm 1.18 = 14.5 \text{ to } 12.2\ \mu m\ (0.572 \times 10^{-3} \text{ to } 0.48 \times 10^{-3}\ in.)$$

(2) Potential error in frequency (signal from sine converter to X-Y-Y' plotter (observed value, N = 24 000 cycles/min):

$$N_e = 24\ 000 \text{ cycles/min} \times \pm 0.0045 = \pm 108 \text{ cycles/min}$$

$$N_e = 24\ 108 \text{ to } 23\ 892 \text{ cycles/min}$$

(3) Potential error in phase angle, from phase meter to X-Y-Y' plotter (observed phase angle, 171°):

$$\varphi_e = 171^\circ \times \pm 0.0028 = \pm 0.479^\circ$$

$$\varphi_e = 171.5^\circ \text{ to } 170.5^\circ$$

(4) Potential error in initial clearance setting from proximity sensor and digital voltmeter (observed clearance, h = 63.5 μm (0.0025 in.)):

$$h_e = 63.5\ \mu m \times \pm 0.0056 = \pm 0.356\ \mu m\ (\pm 1.4 \times 10^{-5}\ in.)$$

$$h_e = 63.86 \text{ to } 63.14\ \mu m\ (0.00251 \text{ to } 0.00249\ in.)$$

To this value must be added the possible misalinement error of ±5.08 μm (±0.0002 in.):

$$h_e = 63.86 \pm 5.08 = 68.94 \text{ to } 58.78\ \mu m\ (0.00271 \text{ to } 0.00231\ in.)$$

Taking a combination of measured values that would give the highest and lowest possible errors results in dimensionless damping values that could be 49 percent too high or 31 percent too low.

The following sample calculations illustrate the variations in the experimental values of damping, stiffness, and squeeze numbers:

Damping coefficient, B:

$$B = \frac{2.79\times10^{-6}\ N \sin \varphi}{e} \qquad \frac{N\text{-sec}}{m}$$

$$B = 62.5\times10^{-8}\ \frac{N \sin \varphi}{e} \qquad \frac{lb\text{-sec}}{in.}$$

e_e = 14.5 to 12.2 μm (0.572×10^{-3} to 0.48×10^{-3} in.)

N_e = 24 108 to 23 892 cycles/min

φ_e = 171.5^o to 170.5^o

h_e = 68.9 to 58.7 μm (0.00271 to 0.00231 in.)

Substituting the positive and negative error values into the equation for damping coefficient gives

$$B_e = 908 \text{ to } 676 \text{ N-sec/m } (5.18 \text{ to } 3.86 \text{ lb-sec/in.})$$

as compared to the nominal value of 776 newton-seconds per meter (4.43 lb-sec/in.).

Dimensionless damping, $\bar{B}$:

$$\bar{B} = \frac{Bh^3}{\mu L^4}$$

$\mu = 1.81\times10^{-5}$ N-sec/m^2 (2.62×10^{-9} lb-sec/$in.^2$)

L = 7.62 mm (3 in.)

Substituting the values into the equation gives

$$\bar{B}_e = 0.486 \text{ to } 0.224$$

as compared to the nominal value of 0.326.

Squeeze number, σ:

$$\sigma = \frac{12\mu\omega L^2}{h^2 P_a} = \frac{2.96\times10^{-8} N}{h^2 P_a}$$

N_e = 24 108 to 23 892 cycles/min

h_e = 68.9 to 58.7 μm (0.00271 to 0.00231 in.)

P_a = 98 289 N/m^2 (14.25 psia)

Substituting the values gives

$$\sigma = 9.38 \text{ to } 6.76$$

as compared to the nominal value of 7.98.

Instrumentation errors in the experimental values of stiffness could result in values that are greater by 22 percent and lower by 23.8 percent. Error values of measured amplitude, phase angle, frequency, and initial clearance are given again as follows:

$$e_e = 19.5 \text{ to } 12.2 \ \mu\text{m} \ (0.572\times10^{-3} \text{ to } 0.48\times10^{-3} \text{ in.})$$

$$N_e = 24\,108 \text{ to } 23\,892 \text{ cycles/min}$$

$$\varphi_e = 171.5^\circ \text{ to } 170.5^\circ$$

$$h_e = 68.9 \text{ to } 58.7 \ \mu\text{m} \ (0.00271 \text{ to } 0.00231 \text{ in.})$$

Substituting these values into the expression for stiffness coefficient,

$$K = \frac{2(U\omega^2)\cos\varphi}{3e} + \frac{2M\omega^2}{3} \qquad \frac{N}{m}\left(\frac{lb}{in.}\right)$$

results in values of

$$K_e = 87.3\times10^5 \text{ to } 63.7\times10^5 \text{ N/m } (49\,843 \text{ to } 36\,362 \text{ lb/in.})$$

as compared to the nominal value of 77.3×10^5 newtons per meter (44 142 lb/in.).

Dimensionless stiffness is defined as

$$\bar{K} = \frac{Kh}{L^2 P_a \left[(P_s/P_a) - 1 \right]}$$

Substituting the values of error values of K_e into this equation gives values of dimensionless stiffness of

$$\bar{K}_e = 1.05 \text{ to } 0.655$$

as compared to the nominal value of 0.86. The following, taken from reference 13, is offered as an explanation for the disagreement between the experimental values of damping and those predicted by the theory of reference 11. For a self-acting gas lubricated squeeze-film bearing, the film is effectively incompressible when the normal velocities are relatively low, that is, for low squeeze numbers. This means that the viscous or damping forces predominate. At high relative velocities the film approaches a purely compressible state where there is virtually no fluid flow. This is, however, an externally pressurized bearing. There is always gas flow out over the sill (regardless of squeeze number), and, therefore, the measured damping does not decrease as rapidly as predicted. The analysis of reference 11 is based on a small perturbation linearized solution. This assumption, however, would not account for the disagreement since the maximum eccentricity ratio observed in these tests was 0.3.

The explanation given earlier in this discussion for the variance observed between experimental values of damping applies to the film stiffness also (ref. 13): When the velocity of the moving surface is relatively low and clearances are high (low squeeze number, $\sigma \rightarrow 0$), the film is effectively incompressible with high viscous forces. This, of course, applies for a pure hydrodynamic bearing and is not completely true for an externally pressurized bearing of the type being considered.

At very small clearances and high approach velocities a somewhat compressible film state exists where the hydrodynamic component of the flow is reduced. This condition results in much greater stiffness values than the theory is capable of predicting.

For the smaller clearance and a supply pressure ratio of 2 there is good agreement between theory and experiment. The measured stiffness, however, continues to increase over the range of clearances investigated (25 to 63.5 μm (0.001 to 0.0025 in.)) whereas the predicted stiffness peaks and then drops off. Where the theory shows a significant increase in film stiffness when the supply pressure ratio is increased from 2 to 3, the measured stiffness increase is only moderate.

COMPARISON BETWEEN OIL AND GAS FILM DAMPER

One of the objectives of this study was to determine the feasibility of using an inherently compensated, externally pressurized, gas film bearing as a flexible damped support. The test apparatus was designed to provide the capability of readily changing both the stiffness and damping characteristics without shutting down the drive system. Control was provided of both the supply air to the pads and the initial clearance by a micrometer adjustment.

Figures 11 and 12 show the variations, both experimental and predicted, in damping coefficients of a single pad for a range of clearances. Average values of the measured damping for a single pad range from a high of 3294 newton-seconds per meter (18.8 lb-sec/in.) at a supply pressure ratio of 3 and a clearance of 25 micrometers (0.001 in.) down to 561 newton-seconds per meter (3.2 lb-sec/in.) at a clearance of 25 micrometers (0.0025 in.) and a supply pressure ratio of 2.

It was suggested in the INTRODUCTION that an externally pressurized gas film damper of the type investigated might find application in small, lightweight turbocompressors. It could be used where bearing compartment temperatures were so high so as to preclude using either oil or elastomers in energy dissipation devices. The calculations that follow show that the type of gas film damper tested can provide sufficient damping to make it a candidate for replacing the oil squeeze-film damper. The oil damper dimensions and the amount of support damping required were calculated for a small, lightweight turborotor simulator (described in ref. 14). This simulator is required to operate above its first bending critical speed with an unbalance of 2.88×10^{-4} kilogram-meter (0.4 oz-in.).

The rotor weighs 5.68 kilograms (12.52 lb) and is supported in two ball bearings. This amount of unbalance is large for a rotor of this weight; however, it represents an unbalance condition that could result if the original balance changed because of blade erosion or wear of machine components.

The equation for dimensionless damping of an incompressible lubricant was obtained from reference 15:

$$\bar{B} = BC_R^3/2\mu L_R^3$$

where

$\bar{B}$ dimensionless damping for oil damper at $\epsilon = 0.4$

L damper length, 0.01 m (0.45 in.)

R damper radius, 0.04 m (1.56 in.)

μ absolute oil viscosity, 0.12 N-sec/m^2 (1.73×10^{-6} lb-sec/in.^{2})

C_R damper clearance, 127 μm (0.005 in.)

Substituting these values into the previous expression and solving for the damping coefficient give a $\bar{B}$ value of 1405 newton-seconds per meter (8.02 lb-sec/in.).

A supply pressure ratio P_s/P_a of 3, a squeeze number of 10, and a clearance of 38 micrometers (0.0015 in.) give a damping coefficient of 1174 newton-seconds per meter (6.7 lb-sec/in.) as shown in figure 12. This value of the damping coefficient is for a single pad only. If three pads are used as arranged in figure 5, the total damping coefficient would be 1.5×1174 or 1840 newton-seconds per meter (10.05 lb-sec/in.). Thus, the air film damper would provide sufficient damping for the application although as presently designed the damper is larger and the clearances are much smaller.

SUMMARY OF RESULTS

Experimental values of damping and stiffness for an externally pressurized, inherently compensated, air film damper were determined for clearances of 63.5, 50.8, 38.1, and 25 micrometers (0.0025, 0.002, 0.0015, and 0.001 in.) at frequencies up to 36 000 cycles per minute and supply pressure ratios of 2 and 3. The damper was 76.2 millimeters (3 in.) square and contained 20 equally spaced feed holes 1.4 millimeters (0.059 in.) in diameter. The test apparatus had three such pads arranged in an equilateral triangular pattern so that the air film in each pad could be excited by a rotating unbalance force.

Measured squeeze film damping coefficients for a single bearing ranged from a high of 3294 newton-seconds per meter (18.8 lb-sec/in.) at a clearance of 25 micrometers (0.001 in.) and a supply pressure ratio of 3 down to 67.1 newton-seconds per meter (3.2 lb-sec/in.) at a clearance of 63.5 micrometers (0.0025 in.) and a supply pressure ratio of 2.

The experimental damping values at a supply pressure ratio of 2, clearances of 63.5 and 50.8 micrometers (0.0025 and 0.002 in.), and squeeze numbers less than 20 are considerably higher than those predicted by a small pressure perturbation theory. At clearances of 38.1 and 25 micrometers (0.0015 and 0.001 in.) the measured damping is less than that predicted by theory. At a supply pressure ratio of 3 the measured damping is again greater than that predicted at high clearances and squeeze numbers less than 20. Agreement is significantly better, however, at clearances of 38.1 and 25 micrometers (0.0015 and 0.001 in.) and relatively high squeeze numbers.

Measured values of the squeeze-film stiffness ranged from a low of 13.1×10^5 newtons per meter (7500 lb/in.) at a clearance of 25 micrometers (0.001 in.) and a supply pressure ratio of 2 to a high of 143.7×10^5 newtons per meter (82 000 lb/in.) at a

clearance of 63.5 micrometers (0.0025 in.) and at a supply pressure ratio of 3.

Measured values of the stiffness coefficient are generally in poor agreement with the theoretical values, particularly at high clearances and low squeeze numbers; that is, they are much less than the predicted values. As was the case with the damping coefficients, the measured stiffnesses at small clearances and high squeeze numbers showed significantly better agreement although they were slightly higher than predicted.

The present damper design provides a damping coefficient of 1840 newton-seconds per meter (10.05 lb-sec/in.) for a pressure ratio of 3, a clearance of 38 micrometers (0.0015 in.), and a squeeze number of 10. This compares with 1405 newton-seconds per meter (8.02 lb-sec/in.) for a previously designed oil squeeze-film damper with a similar diameter.

Results of an error analysis showed that values of the experimental dimensionless damping could be 49 percent higher or 31 percent lower than the nominal value. Values of dimensionless stiffness could be higher than the nominal value by 22 percent or lower by 23.8 percent.

Lewis Research Center,
National Aeronautics and Space Administration,
Cleveland, Ohio, February 26, 1975,
505-04.

REFERENCES

1. Kirk, R. G.; and Gunter, E. J.: Effect of Support Flexibility and Damping on the Dynamic Response of a Single Mass Flexible Rotor in Elastic Bearings. NASA CR-2083, 1972.

2. Lund, Jorgen W.: The Stability of an Elastic Rotor in Journal Bearings with Flexible, Damped Supports. J. Appl. Mech., ASME Trans., vol. 32, ser. E, no. 4, Dec. 1965, pp. 911-920.

3. Rieger, Neville F.: Unbalance Response of an Elastic Rotor in Damped Flexible Bearings at Super Critical Speeds. J. Eng. for Power, ASME Trans., vol. 93, ser. A, Apr. 1971, pp. 265-278.

4. Hays, Donald F.: Squeeze Films for Rectangular Plates. J. Basic Eng., ASME Trans., vol. 85, ser. D, no. 2, June 1963, pp. 243-246.

5. Salbu, E. O. J.: Compressible Squeeze Films and Squeeze Bearings. J. Basic Eng., ASME Trans., vol. 86, ser. D, no. 2, June 1964, pp. 355-366.

6. Licht, L.; and Cooley, J. W.: Dynamics of Externally-Pressurized Sliders with Incompressible and Compressible Films. J. Basic Eng., ASME Trans., vol. 86, ser. D, no. 2, June 1964, pp. 396-404.

7. Tully, N.: Damping in Externally Pressurized Gas Bearing Journals. The Engineer, vol. 222, Nov. 1966, pp. 794-797.

8. Design of Gas Bearings. Vol. 1, Design Notes Mechanical Technology, Inc., 1966.

9. Stiffler, A. K.: Analysis of the Stiffness and Damping of an Inherently Compensated, Multiple Inlet, Circular Thrust Bearing. ASME Trans., vol. 96, ser. F, no. 3, July 1974, pp. 329-336.

10. Mullan, P. J.; and Richardson, H. H.: Plane Vibration of the Inherently Compensated Gas Journal Bearing; Analysis and Comparison with Experiment. ASLE Trans., vol. 7, no. 3, July 1964, pp. 277-287.

11. Stiffler, A. K.; and Smith, D. M.: Dynamic Characteristics of an Inherently Compensated, Square, Gas Film Damper. ASME Trans., vol. 97, ser. F, no. 1, Jan. 1975, pp. 52-62.

12. Thompson, W. T.: Vibration Theory and Applications. Prentice Hall, Inc., p. 52.

13. Gross, William A.: Gas Film Lubrication. John Wiley and Sons, Inc., 1962, p. 307.

14. Cunningham, Robert E.; Gunter, Edgar J., Jr.; and Fleming, David P.: Design of an Oil Squeeze Film Damper Bearing for a Multimass Flexible-Rotor Bearing System. NASA TN D-7892, 1975.

15. Barrett, L. E.; and Gunter, E. J.: Steady State and Transient Analysis of a Squeeze Film Damper for Rotor Stability. ME-4040-114-73U, University of Virginia, 1973.

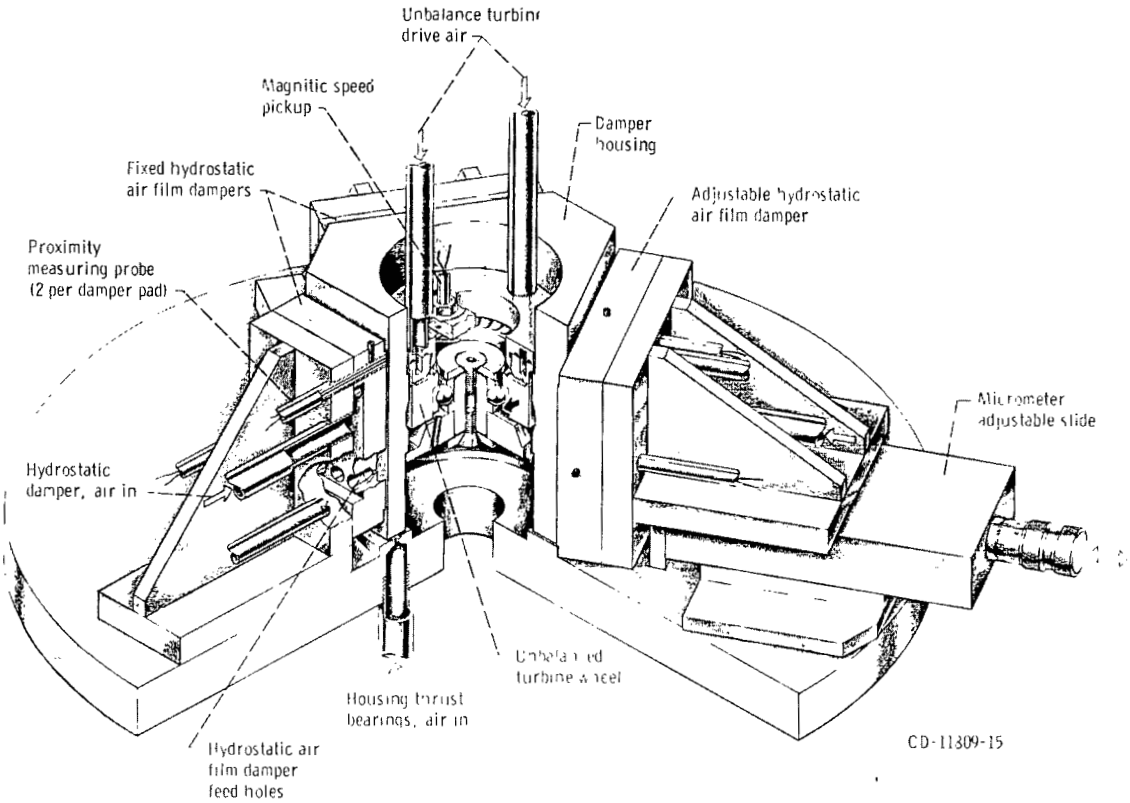

Figure 1. - Test apparatus for hydrostatic, compressible fluid, squeeze damping studies.

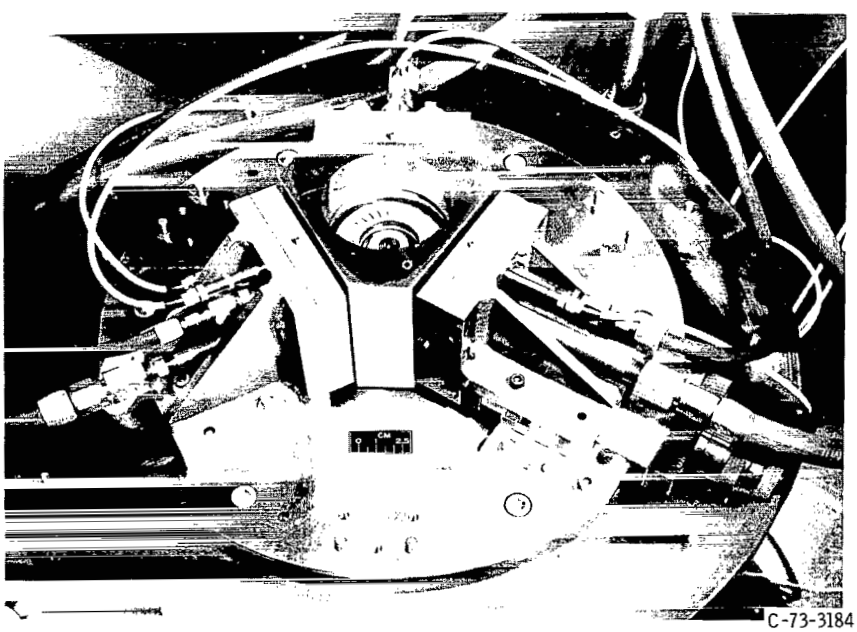

Figure 2. - Squeeze film damping and stiffness test apparatus.

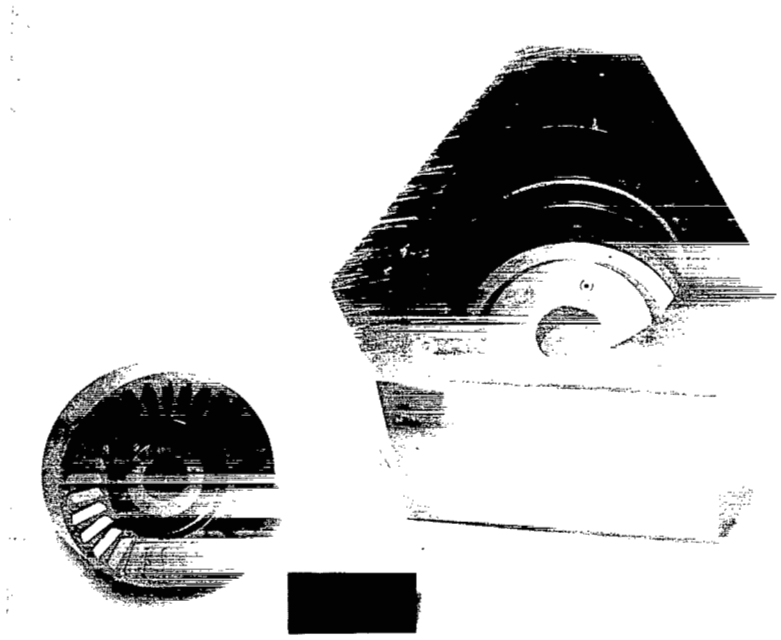

C-73-3182

Figure 3. - Turbine wheel and housing of squeeze film damping and stiffness test apparatus.

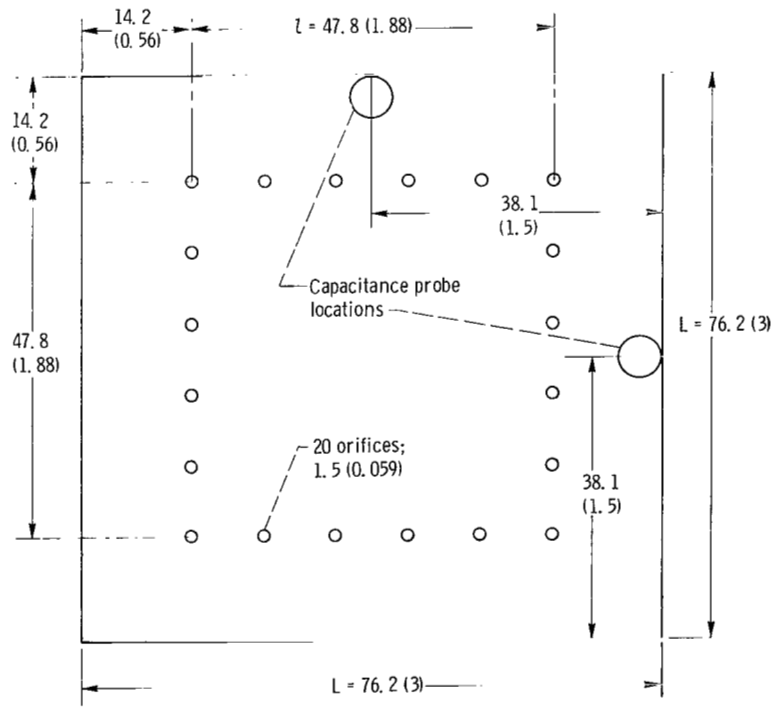

Figure 4. - Hydrostatic air damper pad. (All dimensions are in mm(in.).)

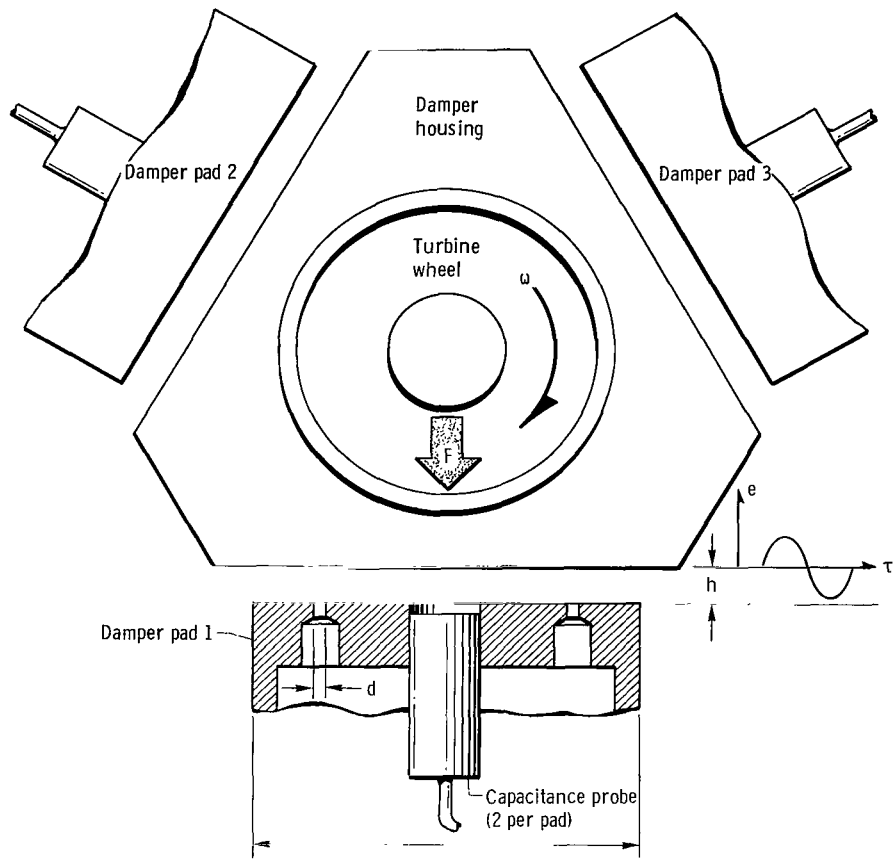

Figure 5. - Schematic of three-pad air squeeze-film damper.

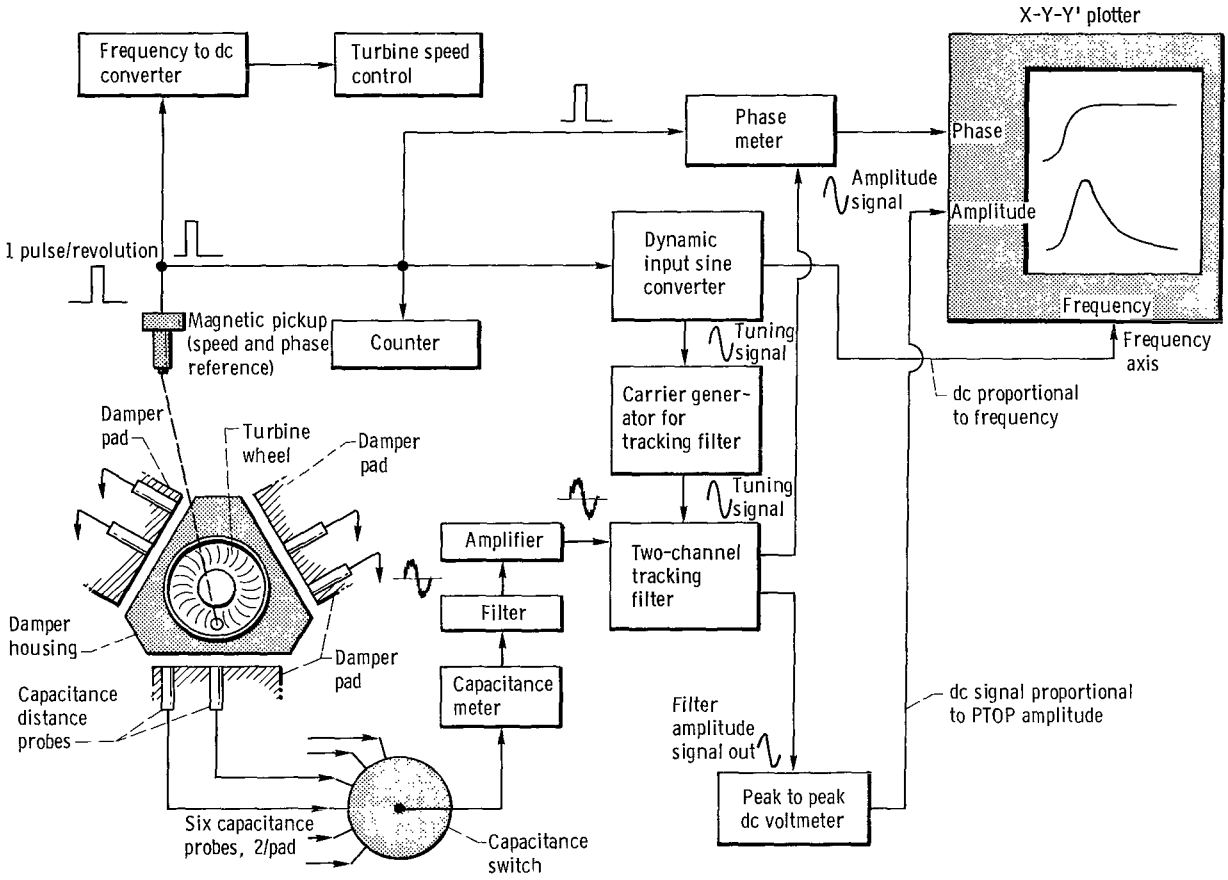

Figure 6. - Instrumentation schematic for air squeeze-film damping studies.

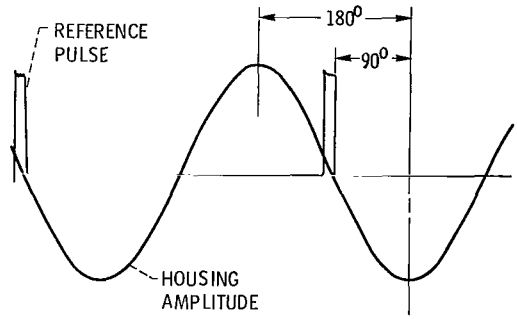

(a) Turbine frequency, 9500 cycles per minute; phase angle from meter, 90°.

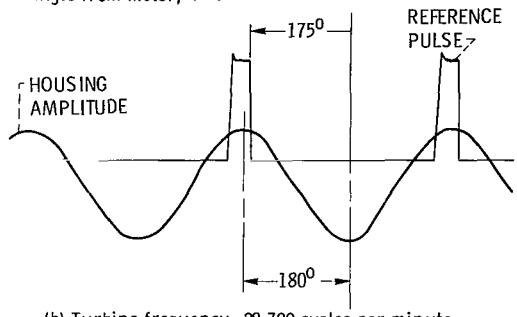

(b) Turbine frequency, 28 700 cycles per minute; phase angle from meter, 175°.

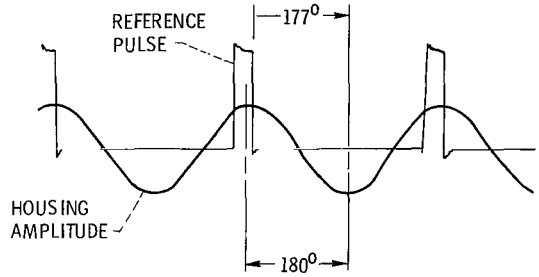

(c) Turbine frequency, 30 500 cycles per minute; phase angle from meter, 177°.

Figure 7. - Phase relationship of position of exciting force and housing displacement.

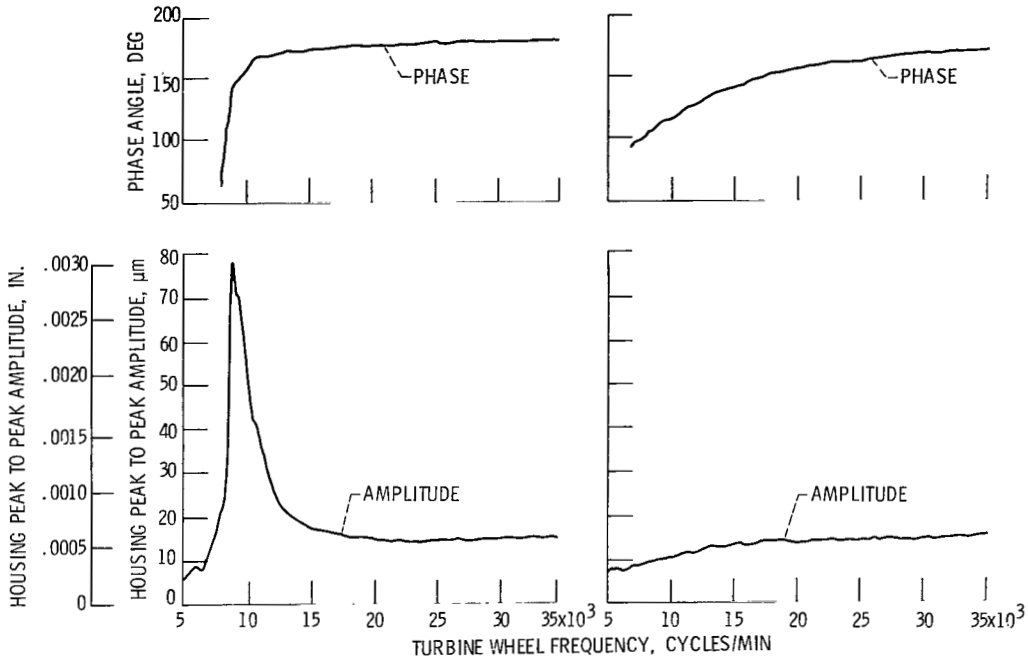

(a) Film thickness, h, 63.5 micrometers (0.0025 in.).

(b) Film thickness, h, 25 micrometers (0.001 in.).

Figure 8. - Housing peak to peak amplitude and phase angle as functions of turbine wheel frequency. Supply pressure ratio, P_s/P_a, 2.

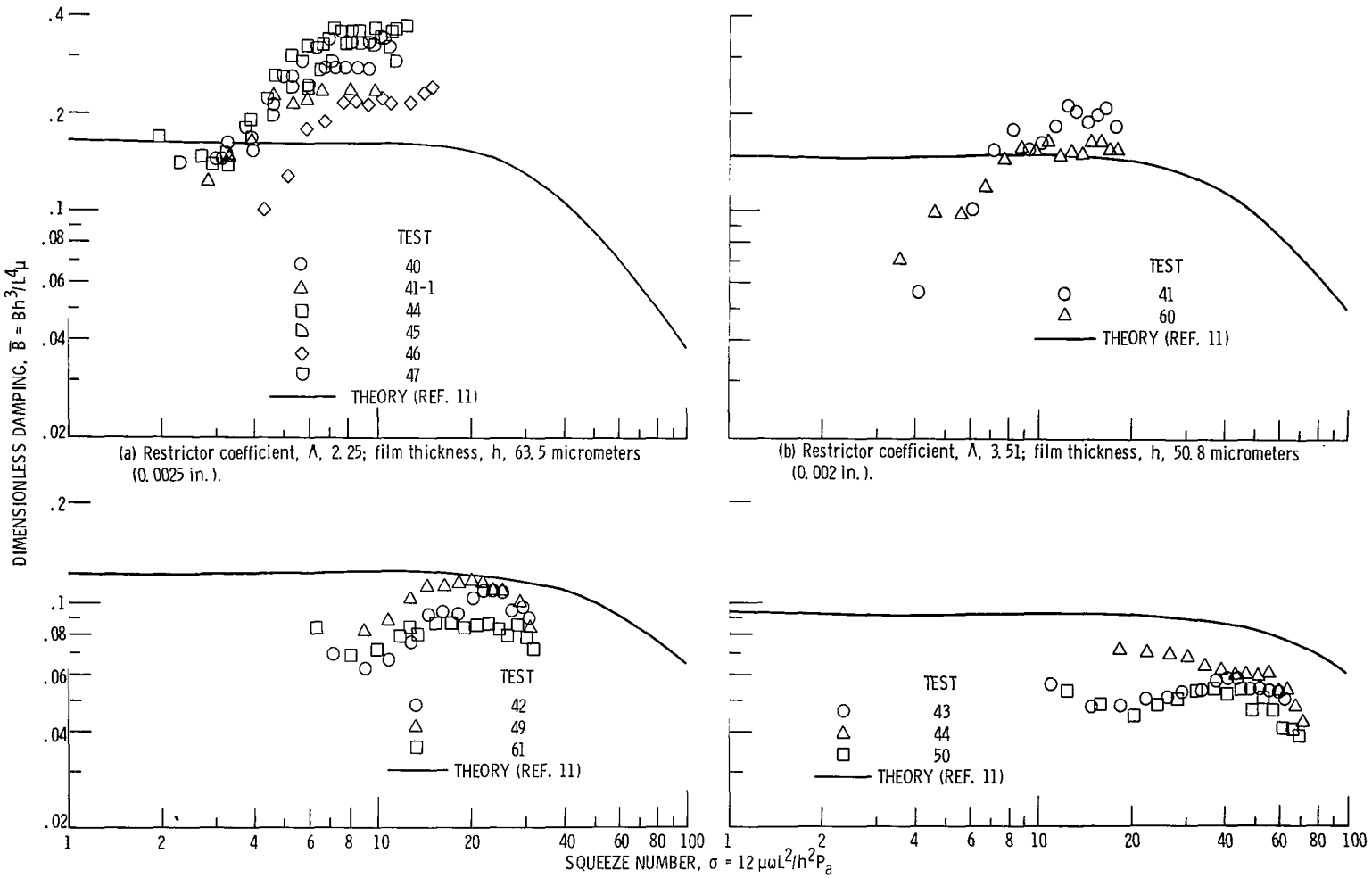

(a) Restrictor coefficient, Λ, 2.25; film thickness, h, 63.5 micrometers (0.0025 in.).

(b) Restrictor coefficient, Λ, 3.51; film thickness, h, 50.8 micrometers (0.002 in.).

(c) Restrictor coefficient, Λ, 14; film thickness, h, 25 micrometers (0.0015 in.).

(d) Restrictor coefficient, Λ, 6.25; film thickness, h, 38.1 micrometers (0.001 in.).

Figure 9. - Dimensionless damping as function of squeeze number for single pad. Supply pressure ratio, P_s/P_a, 2; ratio of center region length to total damper pad length, A, 0.6.

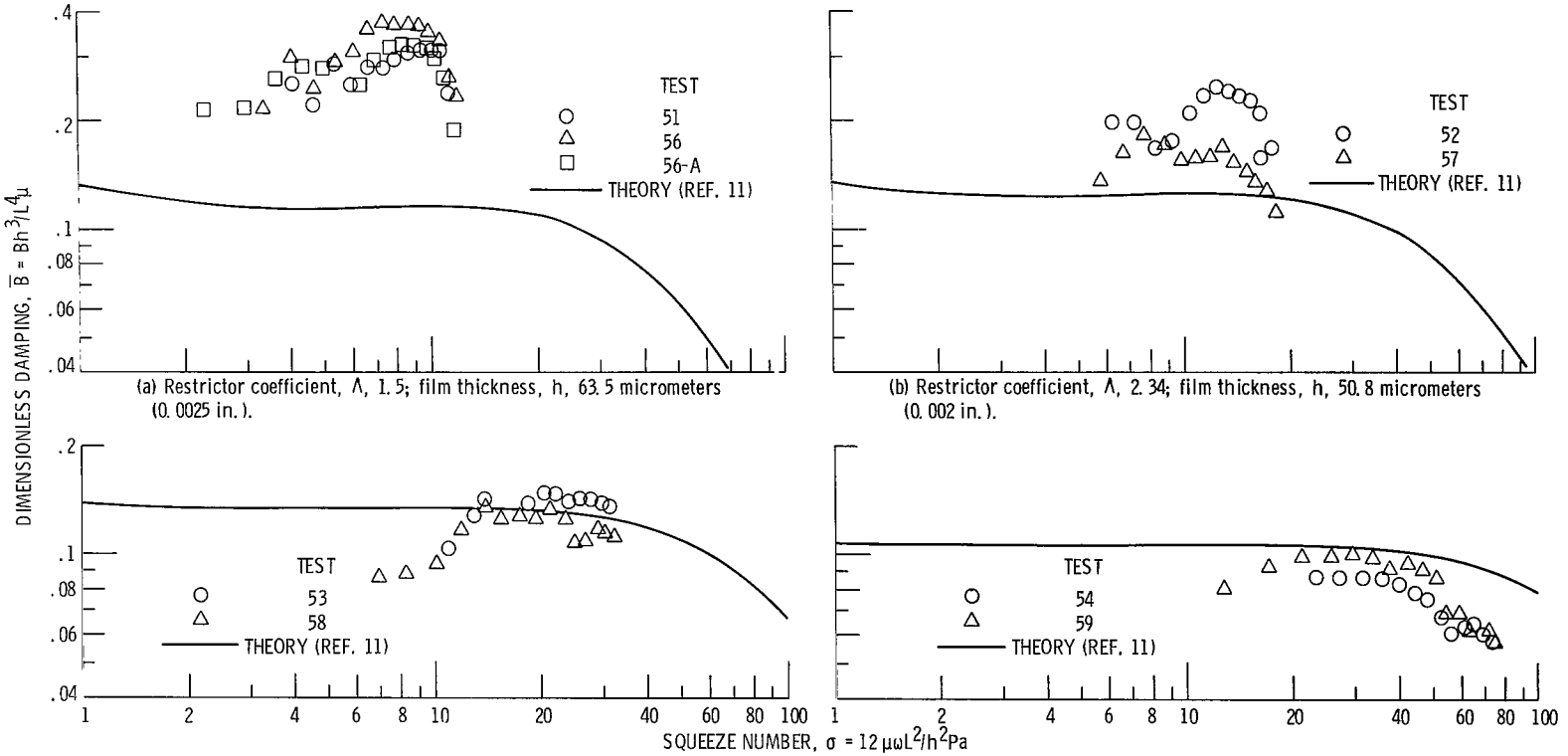

(a) Restrictor coefficient, Λ, 1.5; film thickness, h, 63.5 micrometers (0.0025 in.).

(b) Restrictor coefficient, Λ, 2.34; film thickness, h, 50.8 micrometers (0.002 in.).

(c) Restrictor coefficient, Λ, 4.17; film thickness, h, 38.1 micrometers (0.0015 in.).

(d) Restrictor coefficient, Λ, 9.35; film thickness, h, 25 micrometers (0.001 in.).

Figure 10. - Dimensionless damping as function of squeeze number for single pad. Supply pressure ratio, P_s/P_a, 3; ratio of center region length to total damper pad length, A, 0.6.

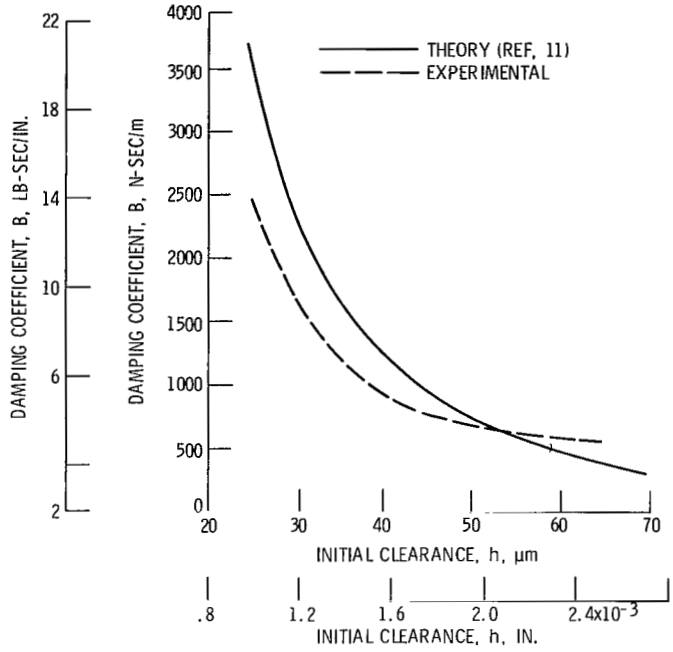

Figure 11. - Squeeze film damping as function of clearance. Supply pressure ratio, P_s/P_a, 2; squeeze number, σ, 10.

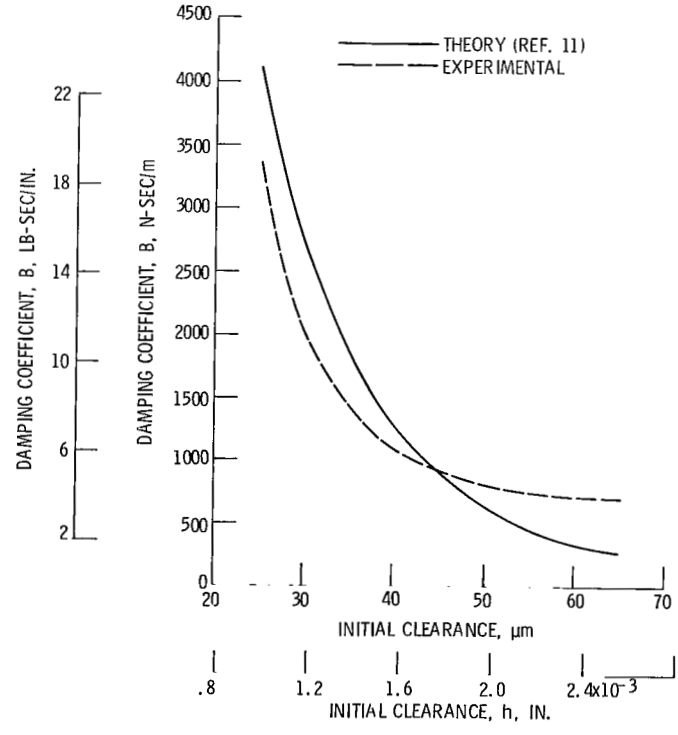

Figure 12. - Squeeze film damping as function of clearance. Supply pressure ratio, P_s/P_a, 3; squeeze number, σ, 10.

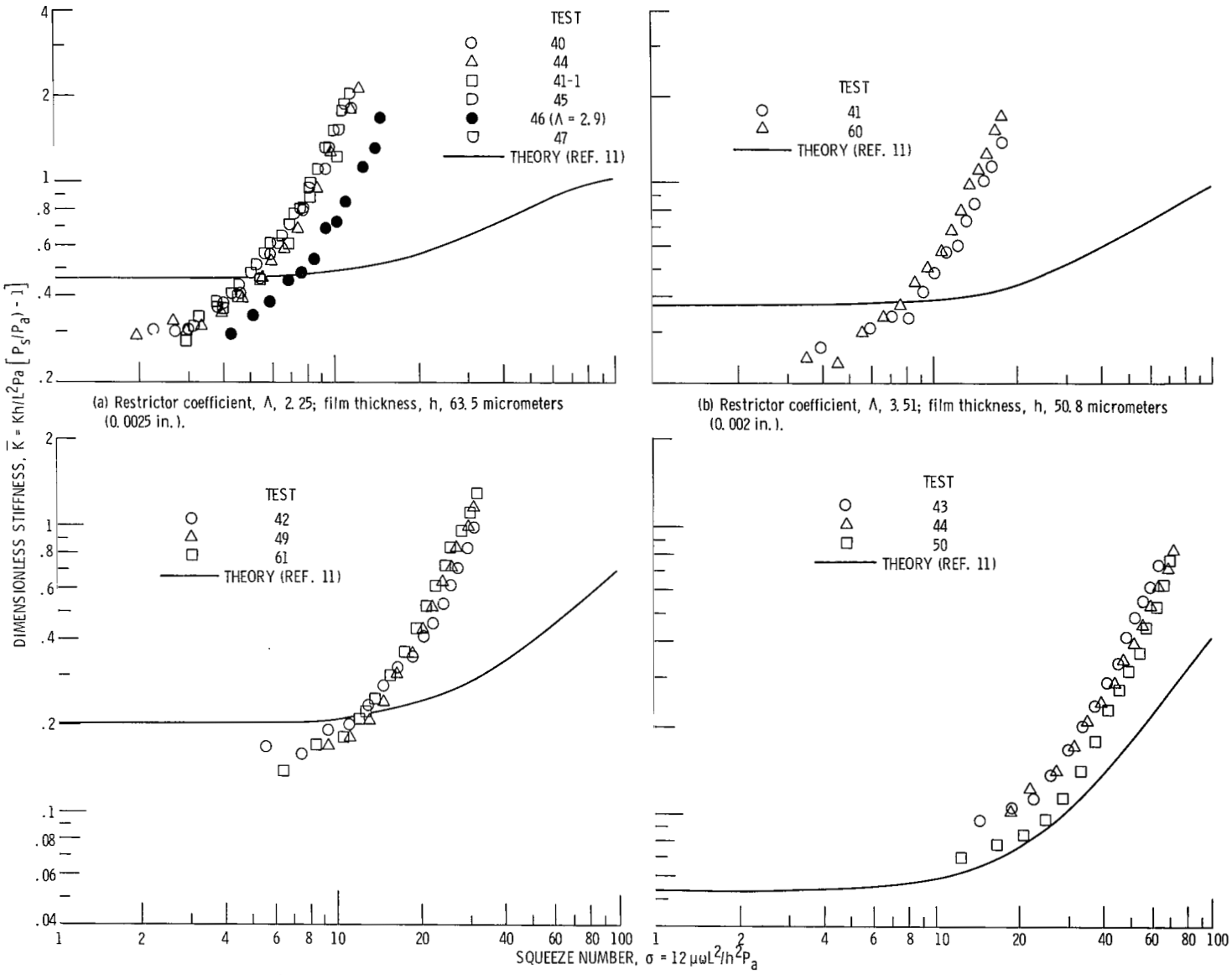

(a) Restrictor coefficient, Λ, 2.25; film thickness, h, 63.5 micrometers (0.0025 in.).

(b) Restrictor coefficient, Λ, 3.51; film thickness, h, 50.8 micrometers (0.002 in.).

(c) Restrictor coefficient, Λ, 6.25; film thickness, h, 38.1 micrometers (0.0015 in.).

(d) Restrictor coefficient, Λ, 14.0; film thickness, h, 25 micrometers (0.001 in.).

Figure 13. - Dimensionless stiffness as function of squeeze number for single pad. Supply pressure ratio, P_s/P_a, 2; ratio of center region length to total damper pad length, A, 0.6.

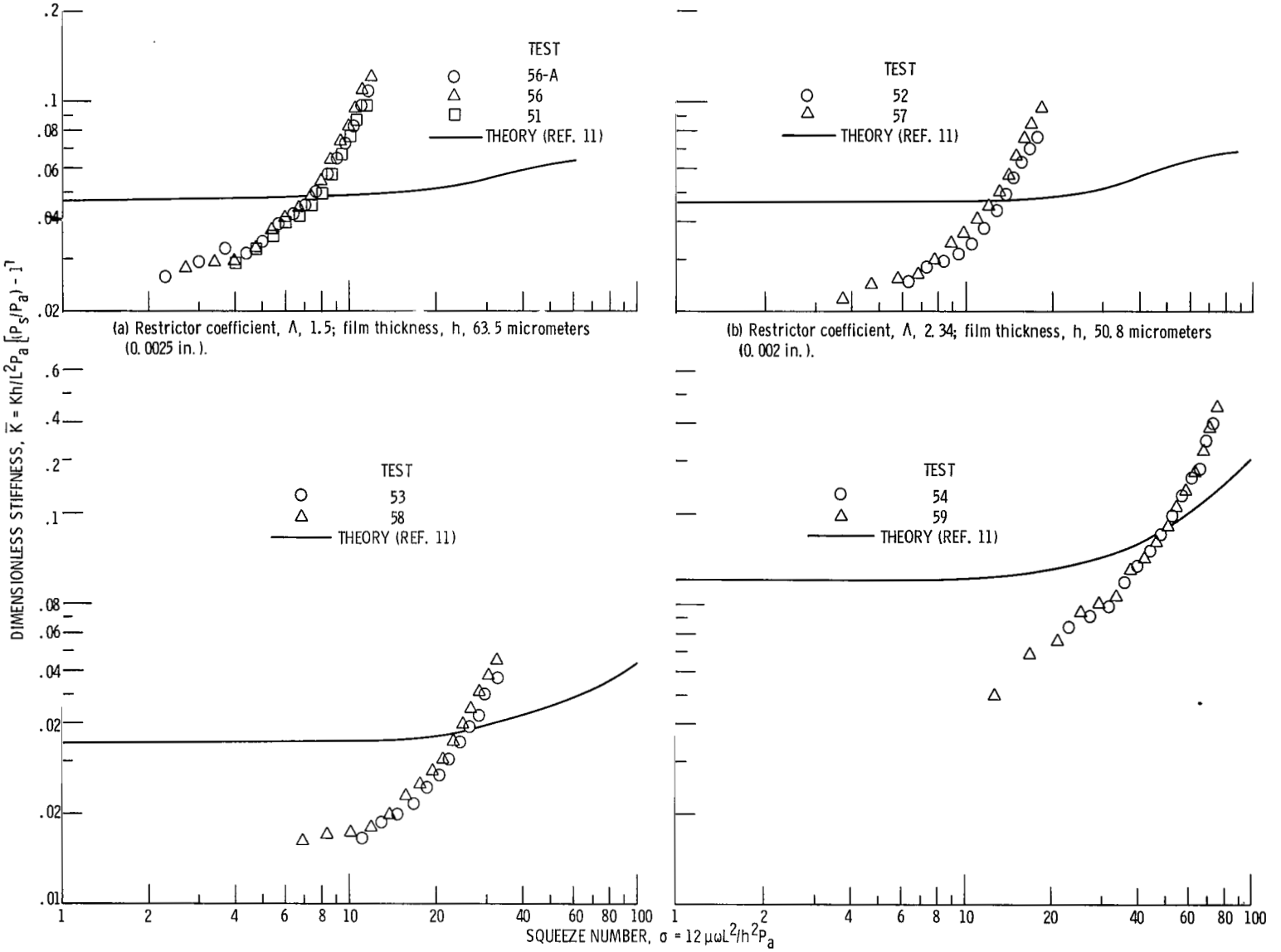

(a) Restrictor coefficient, Λ, 1.5; film thickness, h, 63.5 micrometers (0.0025 in.).

(b) Restrictor coefficient, Λ, 2.34; film thickness, h, 50.8 micrometers (0.002 in.).

(c) Restrictor coefficient, Λ, 4.17; film thickness, h, 38.1 micrometers (0.0015 in.).

(d) Restrictor coefficient, Λ, 9.35; film thickness, h, 25 micrometers (0.001 in.).

Figure 14. - Dimensionless stiffness as function of squeeze number for single pad. Supply pressure ratio, P_s/P_a, 3; ratio of center region length to total damper pad length, A, 0.6.

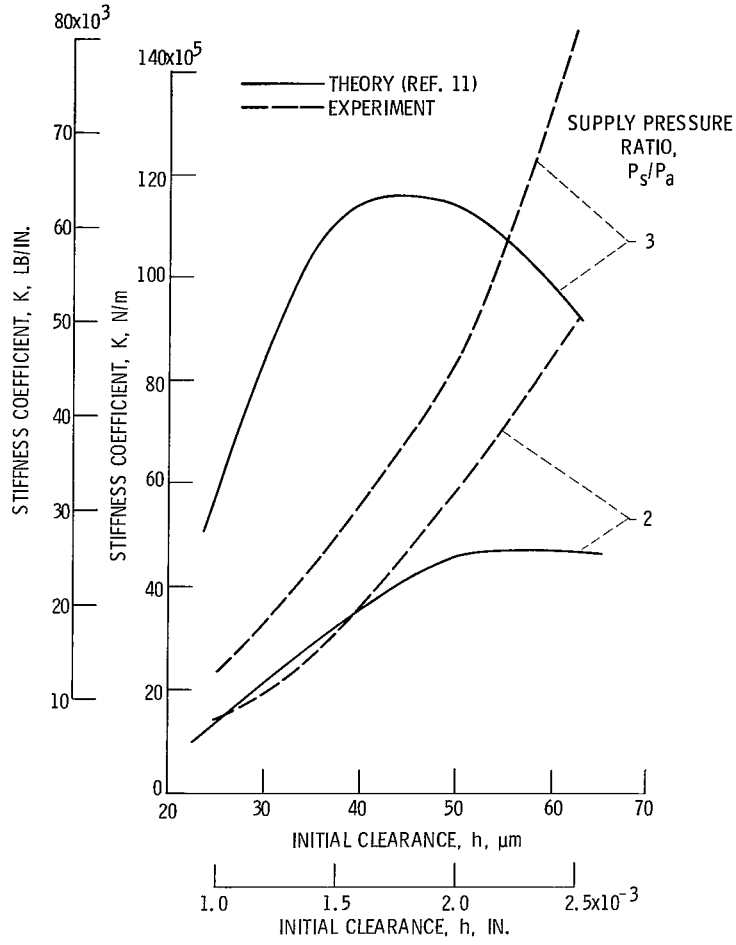

Figure 15. - Stiffness coefficient as function of initial clearance at squeeze number σ of 10.